Quenching and excitation transfers in $n=3$ lithium sublevels

C. Chaleard, B. Dubreuil, and A. Catherinot
Groupe de Recherches sur l'Energétique des Milieux Ionisés, Université d'Orléans, Centre National de la Recherche Scientifique, 45046, Orleans Cedex, France
(Received 3 March 1982)

Quenching and excitation-transfer processes involving the 3^2P and 3^2D states of the Li atom are studied in a temperature-controlled heat-pipe oven with the use of two-step laser excitation of the 4^2S state followed by radiative cascade towards the 3^2P state. Numerical identification of the collision-induced $3^2D \rightarrow 2^2P$ fluorescence with a three-level model allows the determination of radiative coefficients and collisional rate coefficients. 4^2S, 3^2D, and 3^2P radiative lifetimes are found to be in agreement with accepted values. Quenching and excitation transfer strongly depend on the colliding atoms. Rate coefficients for the $3^2D \rightarrow 3^2P$ excitation processes induced by Li, He, and Ne ground-state atoms are measured in the ratio 1.05:0.23:0.02 expressed in 10^{-9} sec^{-1} cm^3.

I. INTRODUCTION

Excitation transfers between excited states of alkali atoms induced by collisions with rare-gas atoms were widely studied both theoretically[1-3] and experimentally[4-6] with emphasis on fine-structure-changing collisions and highly excited (Rydberg) states.[7,8]

Whereas recent experimental studies mainly concern heavier alkali atoms, little of the published data involving excited states of lithium is available. This circumstance results certainly from its corrosive behavior and its relatively high melting temperature (454 K). Only very recently Eldward-Berry and Berry succeeded in measuring collision-induced fine-structure transition-rate coefficients in the Li(2^2P_J)—rare-gas systems.[9] They used a stainless-steel cell mounted in a tube furnace operating at a temperature of 555.7 K to produce 5.9×10^9 cm^{-3} lithium atoms. Fluorescence starting from $J=\frac{1}{2}$ and $\frac{3}{2}$ 2^2P sublevels was excited by a narrow-band cw dye laser, and fine-structure transition-rate coefficients were deduced from the ratio of resonance to sensitized (collision-induced) fluorescences.

In this experiment, we use a four-arm temperature-controlled heat-pipe cell to study collision-induced excitation transfers within the $n=3$ lithium sublevels. In particular, rate coefficients for quenching and excitation transfer involving the 3^2D and 3^2P states colliding with ground-state lithium, helium, and neon atoms are determined.

Two-step laser excitation of the 4^2S state followed by the radiative cascade $4^2S \rightarrow 3^2P$ populate the 3^2P state. This extension of the conventional one-step time-resolved laser spectroscopy method is described in the following with the numerical analysis specially developed to extract rate coefficients from the fluorescence relaxation curves.

II. EXPERIMENTAL SETUP

Figure 1 shows a schematic diagram of the experimental apparatus. The lithium vapor is formed in a four-arm stainless steel temperature-controlled heat-pipe oven (3 cm inner diameter, 15 cm length) mounted in a furnace defining a heating zone in the central part and over 4 cm in each arm of the cell. The temperature T is monitored by a Chromel-Alumel thermocouple in contact with the cell and calibrated against an internally mounted thermocouple. This thermocouple was also used to check the uniform temperature distribution in the central part of the cell. Temperature measurement and monitoring are performed with a Pidomat R_1 controller. Cylinders of stainless-steel mesh (4 cm length) are inserted into the four arms providing a spatially uniform lithium distribution.[10-12] Arm ends are strongly cooled by water circulation and closed by a demountable unit connecting the cell to a vacuum system and holding the windows. In the heating zone, lithium metal (92.7 at.% ^{7}Li and 7.3 at. % ^{6}Li) is vaporized and the vapor streams to the cooling zones, where it condenses. Then the liquid flows back within the metal mesh.

For fixed temperature of the vapor T (within 5 K), atomic and dimer partial pressures P_{Li}, P_{Li_2} are

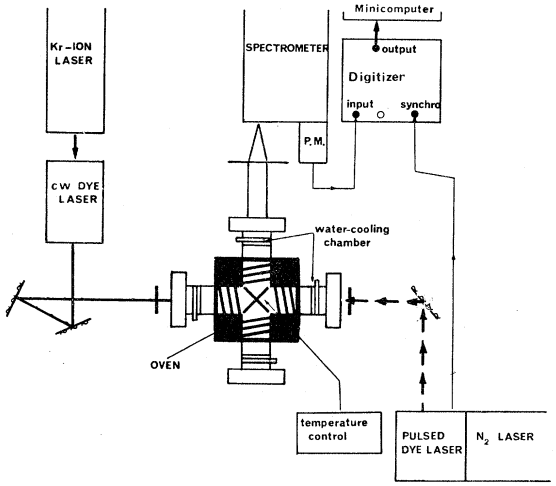

FIG. 1. Experimental setup.

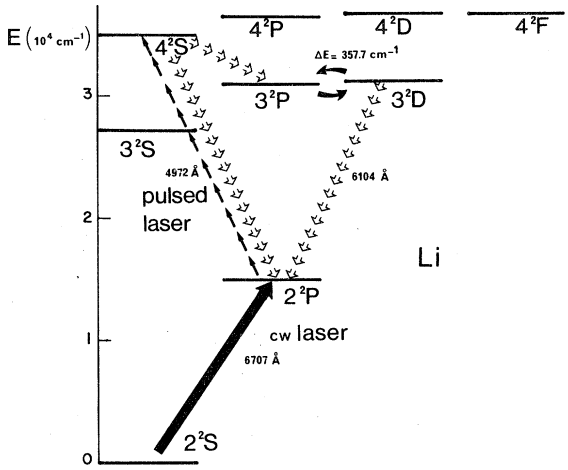

FIG. 2. Partial energy diagram of Li atom involved in the two-step laser excitation of the 4^2S and 3^2P states.

deduced from vapor-pressure data.[13]

The cell is heated in the range 700—950 K giving an atomic Li vapor density in the range $n_{\mathrm{Li}}=4.4\times10^{13}-3.3\times10^{15}$ cm^{-3} and a corresponding dimer density $n_{\mathrm{Li}_2}\cong1.1\times10^{11}-7.3\times10^{13}$ cm^{-3}. Rare gas is added as buffer at pressure P_R ranging independently between 0.1 and 5 torr allowing nearly ideal heat-pipe operation in pure lithium when $P_{\mathrm{Li}}\cong P_R$ or lithium—rare-gas mixture when $P_R > P_{\mathrm{Li}}$. In this case the measured total pressure is $P=P_R+P_{\mathrm{Li}}$. For $P_R < P_{\mathrm{Li}}$ (deduced from vapor-pressure data), the true lithium vapor pressure is fixed by the buffer gas pressure P_R and the vapor is overheated. Satisfactory operation of the cell is no longer possible.

Proper operation of this oven was checked in the $P_R \geq P_{\mathrm{Li}}$ regime by cw laser-induced fluorescence measurements involving the 2^2S-2^2P-3^2D states of Li and is confirmed by the present experiment. Two-step laser excitation is used to populate n^2S or n^2D states ($n>2$) as shown in Fig. 2.

First the 2^2P state is populated from the 2^2S ground state by absorption of the 6708-Å radiation of a cw dye laser (Coherent Inc. model 590 operating with rhodamine 101) pumped by 5 W of an Ar^+ laser (Coherent Inc. model CR 18). The output power of the dye laser can be varied in the range 20—50 mW. The 23-GHz bandwidth exceeds the Doppler width (3.6 GHz) and the 10.2 GHz fine-structure splitting of the $2^2P_{3/2,1/2}\rightarrow2^2S_{1/2}$ line. Before entering one arm of the heat pipe, the cw laser beam is diaphragmed to a diameter of about 1.5 mm. Taking into account absorption of this beam inside the cell[14] one can estimate the population of the 2^2P state to be less than 5×10^{-4} of the 2^2S ground-state population which then can be considered as unperturbed.

The second step involves pulsed excitation of the n^2S or n^2D ($n>2$) states from the 2^2P state by absorption of the radiation emitted by a nitrogen laser pumped tunable dye laser (spectral width of about 12 GHz, pulse width: 3.5 nsec, energy <2 μJ). In these conditions laser saturation and propagation effects on the relaxation of excited-state populations are avoided.[15] After filtering, the beam diameter is about 1.5 mm. The two laser beams travel in opposite directions and are nearly concentric inside the oven.

The resonance or collision-induced fluorescence light is observed at right angles to the laser beams and is imaged by a fused silica onto the slits of a 115-cm grating spectrometer (resolving power ~50 000) and then onto a RCA 7265 photomultiplier tube (rise time: 2 nsec). Time dependence of the output signal is analyzed in this experiment by a 200-MHz Tektronics 7912 AD programmable digitizer (time resolution 1.7 nsec) synchronized with the pulsed laser and connected to a Hewlett Packard (H.P.) 85 minicomputer.

III. EXCITATION TRANSFER IN THE $n=3$ Li SUBLEVELS

A. Experiment

With the two-step laser excitation scheme described in Sec. II, one can populate the 3^2D state from the 2^2P state by pumping the $2^2P\rightarrow3^2D$ tran-

sition ($\lambda_L=6104$ Å). Indeed the resonance fluorescence is observed, but the collision-induced fluorescence (3^2P-2^2S transition, $\lambda=3233$ Å) starting from the neighboring 3^2P level cannot be detected owing to the strong reabsorption by ground-state atoms in the oven.

The direct excitation of the 3^2D state provides only information on its apparent lifetime as deduced from monoexponential analysis of the resonance fluorescence light relaxation. Excitation of the 3^2P state from the 2^2S ground state at $\lambda_L=3233$ Å cannot be performed with the pulsed laser available in this experiment.

To overcome these problems, we use a three-step excitation process involving the 4^2S state to populate the 3^2P state. This excitation process is shown on Fig. 2. The 4^2S state is first populated by the two-step laser excitation scheme $2^2S\rightarrow 2^2P$, $2^2P\rightarrow 4^2S$ ($\lambda_L=4972$ Å). The radiative cascade $4^2S\rightarrow 3^2P$ populates the 3^2P state with a rate of 7.46×10^6 sec^{-1}.[16]

Atomic collisional processes

$$\mathrm{Li}(3^2P)+\mathrm{Li}(2^2S)\rightarrow \mathrm{Li}(3^2D)+\mathrm{Li}(2^2S)-\Delta E\ , \tag{1}$$

$$\mathrm{Li}(3^2P)+R\rightarrow \mathrm{Li}(3^2D)+R-\Delta E\ , \tag{2}$$

(R stands for a ground-state rare-gas atom) transfer part of the 3^2P population to the 3^2D state leading to emission of sensitized fluorescence light in the 3^2D-2^2P transition. The time behavior and the strength of this fluorescence light characterizes the $3^2P\rightarrow 3^2D$ excitation transfer process.

An initial 4^2S level population can also be transferred to the other $n=4$ sublevels by collisional processes

$$\mathrm{Li}(4^2S)+\mathrm{Li}(2^2S)\rightarrow \mathrm{Li}(4^2L)+\mathrm{Li}(2^2S)-\Delta E\ , \tag{3}$$

$$\mathrm{Li}(4^2S)+R\rightarrow \mathrm{Li}(4^2L)+R-\Delta E\ , \tag{4}$$

where $L=P,D$, and F.

But due to the large energy gap ($\Delta E\sim 1500$ cm^{-1}) with respect to the kinetic energy ($kT\leq 650$ cm^{-1}), these processes are inefficient as observed experimentally.

For the same reason, collisional transfers

$$\mathrm{Li}(4^2S)+\{\underset{R}{\mathrm{Li}}(2^2S)\rightarrow \mathrm{Li}(3^2L)+\{\underset{R}{\mathrm{Li}}(2^2S)+\Delta E\ , \tag{5}$$

where $L=S$, P, and D, involving ΔE as large as ~ 5000 cm^{-1}, can be neglected. This was checked on the reverse reaction: $\mathrm{Li}(3^2D)\rightarrow \mathrm{Li}(4^2S)$. In the 3^2D pumping experiment no induced fluorescence light was observed in the 4^2S-2^2P transition.

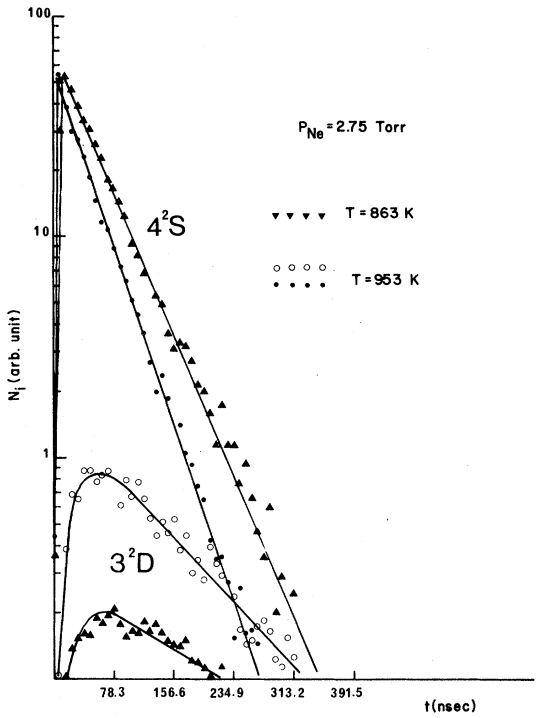

FIG. 3. Time-dependent 4^2S, 3^2D population variations following pulsed laser excitation of the 4^2S level for $P_{Ne}=2.75$ torr and two different oven temperatures $T=953$ and 863 K.

Thus, in our experimental conditions, two-step laser excitation of the 4^2S state leads principally to observation of induced fluorescence in the 3^2D-2^2P transition. However, at higher lithium pressures, weak $4^2D\rightarrow 2^2P$ fluorescence is also detected.

Figures 3 and 4 show some typical experimental recordings of the 4^2S, 3^2D, and 4^2D population relaxations following pulsed laser excitation of the 4^2S state. These relative populations are deduced from the time variation of the recorded fluorescence light after intensity calibration of the detection system.[15]

Figure 3 shows the results of two experiments performed with constant Ne pressure $P_{Ne}=2.75$ torr and two different oven temperatures: $T=953$ K, $n_{Li}=3.33\times 10^{15}$ cm^{-3}, and $T=863$ K, $n_{Li}=4.82\times 10^{14}$ cm^{-3}.

Figure 4 shows the results of two experiments performed with constant oven temperature $T=883$ K, $n_{Li}=7.68\times 10^{14}$ cm^{-3} and two different He pressures: $P_{He}=2.4$ torr, $n_{He}=2.55\times 10^{16}$ cm^{-3}, and $P_{He}=0.9$ torr, $n_{He}=9.07\ 10^{15}$ cm^{-3}.

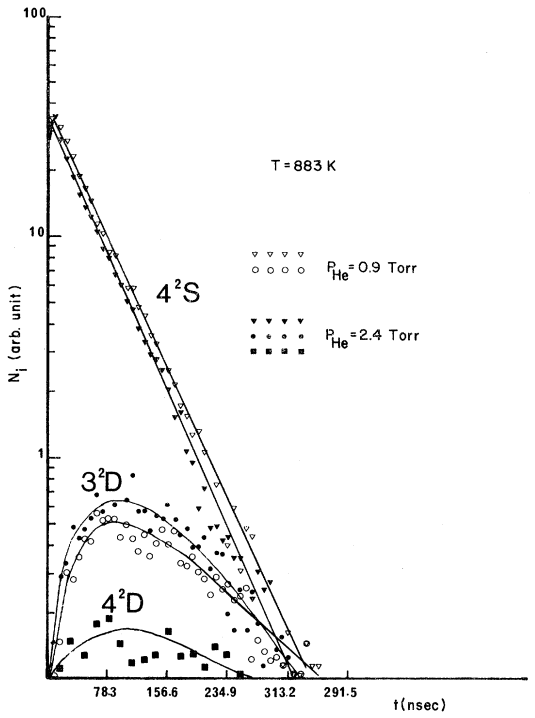

FIG. 4. Time-dependent 4^2S, 3^2D population variations following pulsed laser excitation of the 4^2S level for $T=883$ K and two different He pressures $P_{He}=2.4$ and 0.9 torr.

Qualitative information can be deduced from these figures. Lowering of n_{Li} by a factor ~ 7 leads to a lowering of the transferred 3^2D population for constant initial 4^2S population by a factor ~ 4.5 whereas lowering of n_{He} by a factor ~ 2.8 leads to a lowering of the 3^2D population by a factor ~ 1.2. This indicates that 3^2P-3^2D excitation transfers induced by collisions with Li atoms are certainly more efficient than those induced by He atoms.

B. Quantitative analysis

On the basis of the previous qualitative analysis the population rate equations connecting the 4^2S, 3^2P, and 3^2D levels can be written

$$\frac{dN_1}{dt}=a_{11}N_1+a_{12}N_2 ,$$
$$\frac{dN_2}{dt}=a_{21}N_1+a_{22}N_2+a_{23}N_3 , \quad (6)$$
$$N_1(0)=N_1^0, N_2(0)=N_2^0 ,$$

where $N_1=N_{3^2D}$, $N_2=N_{3^2P}$, and $N_3=N_{4^2S}$.

Furthermore, the free-laser 4^2S relaxation rate equation is

$$\frac{dN_3}{dt}=a_{33}N_3+\sum_{J=4}^{6}a_{3J}N_J ,$$
$$N_3(0)=N_3^0 , \quad (7)$$

where $N_4=N_{4^2P}$, $N_5=N_{4^2D}$, and $N_6=N_{4^2F}$.

In Eqs. (6) and (7) the term a_{ij} $(i\neq j)$ represents the coefficient of the reactions populating the state $|i\rangle$ from state $|j\rangle$. This term has the form

$$a_{ij}=\alpha_{ij}+\beta_{ij}^R n_R+\beta_{ij}^{Li} n_{Li} \quad (8)$$

where α_{ij} is the coefficient of spontaneous transformation from $|j\rangle$ to $|i\rangle$ and β_{ij}^R, β_{ij}^{Li} are the rate coefficients of the excitation-transfer processes Eqs. (1) and (2).

The coefficient a_{23} connecting the 4^2S and 3^2P states represents the radiative cascade $4^2S \rightarrow 3^2P$: $a_{23}=\alpha_{23}=7.46\times 10^6$ sec^{-1}.[16]

The diagonal term a_{ii} corresponds to the quenching coefficient of state $|i\rangle$ and is therefore negative

$$a_{ii}=-\alpha_{ki}-\sum_{j\neq i}a_{ji} , \quad (9)$$

where α_{ki} corresponds to the loss of population from $|i\rangle$ to the outside of the system described by Eqs. (6) and (7): spontaneous emission, associative ionization, molecular quenching, etc.

The unknown population $N_2(N_{3^2P})$ can be eliminated by combining Eqs. (6) and (7). One obtains the second-order rate equation connecting the transferred N_{3^2D} population to the N_{4^2S} source term:

$$A\frac{d^2N_1}{dt^2}-B\frac{dN_1}{dt}+CN_1-N_3=g(A,B,C)=0 ,$$
$$N_1(0)=N_1^0, \left[\frac{dN_1}{dt}\right]_0=\dot{N}_1^0 , \quad (10)$$

where

$$A=1/a_{12}a_{23},$$
$$B=(a_{11}+a_{22})/a_{12}a_{23} , \quad (11)$$
$$C=(a_{11}a_{22}-a_{12}a_{23})/a_{12}a_{23} .$$

Now the problem is to identify A, B, C and therefore a_{12}, a_{11}, a_{22} from measurements of $N_1(t)$.

Such a problem was solved previously in our laboratory in the case of first-order rate equations to provide excitation-transfer rate coefficients in the $n=3$ (Ref. 15) and $n=4$ (Ref. 17) sublevels of helium in a glow discharge.

The method based on optimization algorithms

and named "identification method" allowed us to determine the a_{ij}'s so as to minimize the difference between the experimental $N_i(t)$ values and those calculated from the model.

This method is extended here to the special case of Eq. (10). The identification problem is equivalent to that of finding the minimum of the error function

$$J(A,B,C)=\int_{t_0}^{t_1}[N_1(t)^{\text{expt}}-N_1(t)^{\text{calc}}]^2dt\ ,$$

where $N_1(t)^{\text{calc}}$ are values corresponding to $N_1(t)^{\text{expt}}$ calculated from Eq. (10). As presented in the Appendix, the minimum of $J(A,B,C)$ can be obtained from the iterative gradient algorithm[18]

$$A^{(k+1)}=A^{(k)}-\rho_A^{(k+1)}\left[\frac{\partial J}{\partial A}\right]_k\ ,$$

$$B^{(k+1)}=B^{(k)}-\rho_B^{(k+1)}\left[\frac{\partial J}{\partial B}\right]_k\ ,\quad k=0,1,2,\ldots,$$

$$C^{(k+1)}=C^{(k)}-\rho_C^{(k+1)}\left[\frac{\partial J}{\partial C}\right]_k\ , \tag{12}$$

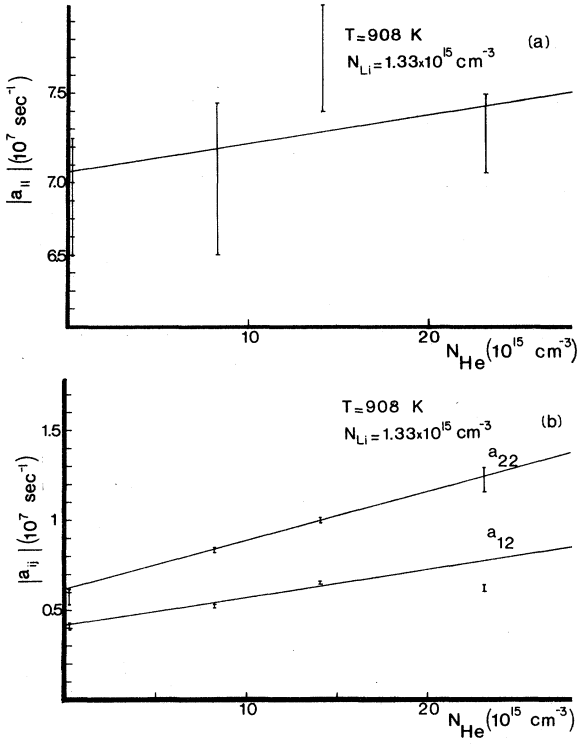

FIG. 5. Transfer coefficients a_{ij} as a function of n_{He} for $T=908$ K: (a)—$a_{11}3^2D$ quenching coefficient; (b)—$a_{22}3^2P$ quenching coefficient and $a_{12}3^2D\rightarrow 3^2P$ transfer coefficient.

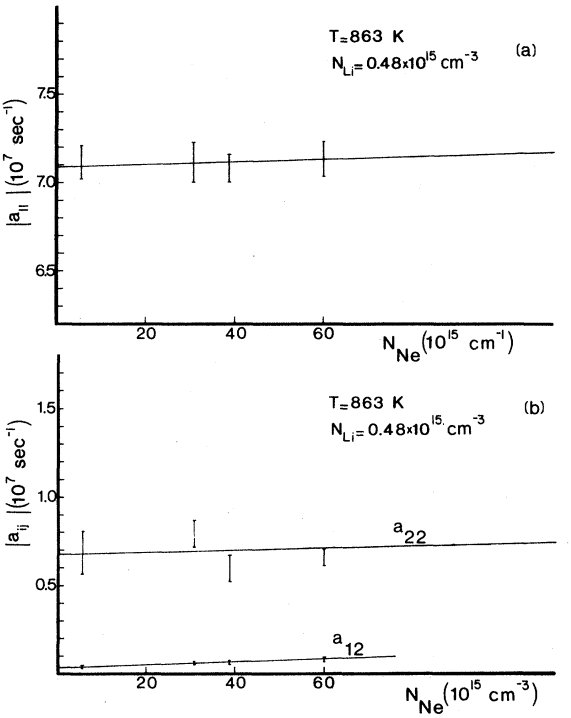

FIG. 6. Transfer coefficients a_{ij} as a function of n_{Ne} for $T=863$ K: (a)—$a_{11}3^2D$ quenching coefficient; (b)—$a_{22}3^2P$ quenching coefficient and $a_{12}3^2D\rightarrow 3^2P$ transfer.

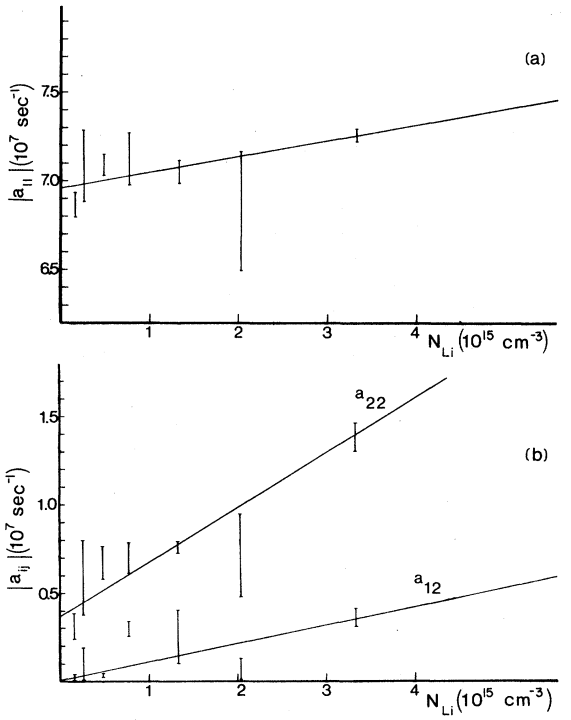

FIG. 7. Transfer coefficients a_{ij} as a function of n_{Li}: (a)—$a_{11}3^2D$ quenching coefficient; (b)—$a_{22}3^2P$ quenching coefficient and $a_{12}3^2D\rightarrow 3^2P$ transfer.

TABLE I. 3^2P, 3^2D, and 4^2S radiative coefficients and lifetimes.

	Spontaneous decay (10^7 sec^{-1})	Lifetime (nsec)
3^2D	6.90±0.32[a]	14.5 ±0.7[a]
	6.85±0.06[b]	14.6 ±0.13[b]
	7.16[c]	13.97[c]
	6.96±0.08 (this work)	14.4 ±0.3 (this work)
3^2P	0.493±0.019[d]	203 ±8[d]
	0.494[c]	202.4[c]
	0.37±0.09 (this work)	270 ±50 (this work)
4^2S	1.75[c]	56.9[c]
	1.76 ±0.03 (this work)	56.8 ±1 (this work)

[a]Reference 19.
[b]Reference 20.
[c]Reference 16.
[d]Reference 21.

where k is the iteration number, $(\partial J/\partial A)_{(k)}$, $(\partial J/\partial B)_{(k)}$, and $(\partial J/\partial C)_{(k)}$ are the functional derivatives (gradients) of the error function, and $\rho_{A,B,C}^{(k+1)}$ are the convergence coefficients measuring the variations of A, B, and C around the minimum of $J(A,B,C)$.

The experimental curves $N_{3^2D}(t)^{\text{expt}}=N_1(t)^{\text{expt}}$ have been identified in this manner to Eq. (10) for five different temperatures of the oven (different n_{Li} values) and for five different rare-gas pressure values.

In each experimental situation (T,P_R), a_{ij} coefficients are deduced from the identified coefficients A, B, and C through relations (11) assuming that a_{12} and a_{21} (i.e., β_{12} and β_{21}) are connected by the microreversibility principle.

The three coefficients a_{11}, a_{22}, and a_{12} are reported in Fig. 5 as a function of n_{He} for $T=908$ K and in Fig. 6 as a function of n_{Ne} for $T=863$ K. Similar results are obtained for the five different T values.

TABLE II. Collisional quenching and transfer rate coefficients measured in the present experiment.

Rate coefficients (10^{-9} sec^{-1}/cm^3)	Li	He	Ne
$\bar{\beta}_{4^2S}$	1.23±0.24	0.062±0.042	~0.016
$\bar{\beta}_{3^2D}$	1.08±0.22	0.18 ±0.09	~0.03
$\bar{\beta}_{3^2P}$	2.8 ±0.26	0.23 ±0.06	~0.02
$\bar{\beta}_{3^2P\text{-}3^2D}$	1.05±0.15	0.23 ±0.1	~0.02

From these curves, $\beta_{ij}^R i$, $j=1$, 2 are determined by linear regression through Eqs. (8) and (9). The intercept with the ordinate axis ($n_R=0$) gives for a fixed oven temperature (n_{Li} value) the sum $S_{ij}=\alpha_{ij}+\beta_{ij}^{\text{Li}}n_{\text{Li}}$. These values deduced from both helium and neon experiments are plotted in Fig. 7 as a function of n_{Li}. The radiative coefficients α_{ij} and the β_{ij}^{Li} rate coefficients are determined by linear regression.

The radiative coefficients and the collisional rate coefficients obtained by this method are reported, respectively, in Tables I and II. The $\bar{\beta}_{ij}$ coefficients are β_{ij} coefficients averaged over the five temperature experiments.

C. Quenching of the 4^2S state

The free relaxation rate equation for N_{4^2S} given by Eq. (7) can be reduced if we take into account the fact that in our experimental conditions the population transferred by collisions to the 4^2P, 4^2D, and 4^2F states is less than 1% of the N_{4^1S} population as shown in Sec. III A (Fig. 4).

In these conditions the repopulating term

$$\sum_J a_{3J}N_J, J=P,D,F\ ,$$

can be neglected in Eq. (7) and N_{4^2S} follows an exponential law as shown experimentally in Figs. 3 and 4. The quenching coefficient a_{33} for given n_{Li} and N_R values is easily determined, and plots of a_{33} vs n_{He}, n_{Ne}, and n_{Li} give as described in Sec. III B the radiative coefficients α_{33} and the quenching rate coefficients $\bar{\beta}_{33}^R$ and $\bar{\beta}_{33}^{\text{Li}}$ of the 4^2S state. These values are, respectively, given in Tables I and II.

IV. DISCUSSION

A. Radiative coefficients

The radiative coefficients

$$\alpha_{11}=A_{3^2D\text{-}2^2P}+A_{3^2D\text{-}3^2P}=\alpha_{3^2P}\ ,$$

$$\alpha_{22}=A_{3^2P\text{-}2^2S}+A_{3^2P\text{-}3^2S}=\alpha_{3^2D}\ ,$$

$$\alpha_{33}=A_{4^2S\text{-}2^2P}+A_{4^2S\text{-}3^2P}=\alpha_{4^2S}\ ,$$

and the lifetimes $\tau_{ii}=1/\alpha_{ii}$ are compared in Table I with values given by different authors. Broad agreement is observed except for the 3^2P value which is found to be lower than the other published values. This fact can be explained as being due to

TABLE III. Comparison of some excitation-transfer cross sections for alkali atoms induced by collisions with ground-state alkali atoms and rare gases.

	Transfers	$\lvert\Delta E\rvert/kT$	Ground-state alkali atom.	Transfer cross section (Å^2) He	Ne	Ar
Li	$3^2P\rightarrow 3^2D$	0.6	43.4 (this work)	8.6 (this work)	1.1 (this work)	
Na	$4^2D\rightarrow 4^2F$	0.11		117.5±32.5[a]	55 ±12.5[a]	32.5 ±10[a]
Rb	$6^2P_{1/2}$-$6^2P_{3/2}$	0.26	245±64[b]			
	$6^2P_{3/2}$-$6^2P_{1/2}$			17.1±3.6[c]	5.6 ±1[c]	13.2 ±2.6[c]
Cs	$7^2P_{1/2}$-$7^2P_{3/2}$	0.51		12 ±2[d]	0.18 ±0.03[d]	0.12 ±0.02[d]
	$7^2P_{3/2}$-$7^2P_{1/2}$			11 ±2[d]	0.16 ±0.03[d]	0.10 ±0.02[d]
				12.8±2.6[c]	0.047±0.01[c]	0.075±0.02[c]
	8^2P quenching		190±63[e]	34 ±11[e]	4.4 ±1.4[e]	5.5 ±1.8[e]

[a]Reference 22.
[b]Reference 23.
[c]Reference 24.
[d]Reference 4.
[e]Reference 25.

the strong self-absorption of the $3^2P\rightarrow 2^2S$ resonance line in the cell. In our experimental conditions, the optical escape factor for this line is $\Lambda\sim 0$ so that spontaneous decay of the 3^2P state is mainly due to the $3^2P\rightarrow 3^2S$ transition. Indeed, the value $A_{3^2P\text{-}3^2S}=3.77\times 10^6$ sec^{-1} given in Ref. 16, agrees with our experimental "apparent" radiative coefficient $\alpha_{22}=3.7\pm 0.9\times 10^6$ sec^{-1}.

B. Collisional processes

From Table II two observations can be made. First, excitation transfers and quenching processes within the 3^2P and 3^2D states and quenching of the 4^2S state strongly depend on the colliding atom. One has

$$\bar{\beta}_{ij}^{\mathrm{Li}}>\bar{\beta}_{ij}^{\mathrm{He}}>\bar{\beta}_{ij}^{\mathrm{Ne}}\ .$$

This behavior was previously observed in fine structure changing collisions involving heavier alkali atoms. For comparison, we have reported in Table III cross sections obtained by different authors in Na, Cs, and Rb for excitation transfers with a $\Delta E/kT$ ratio of the same order of magnitude as for the 3^2P-3^2D transfer in Li ($\Delta E/kT=0.6$).

The difference (one order of magnitude) between He and Ne excitation transfer cross sections was interpreted by Krause[26] in terms of a model describing the rare-gas–alkali-atom interaction as a scattering of the valence electron by the rare gas. This model was supported by relative comparison of the electron–rare-gas scattering cross sections with excitation transfers in Cs (Ref. 25) and Rb.[27]

Furthermore, the magnitude of excitation-transfer cross sections reported in Table III appears to be dependent on the energy gap involved in the transfer. This dependence was observed in different collisional systems and particularly in helium-helium excitation transfers.[15,17]

The second observation concerns the 3^2P Li-collisional quenching coefficient $\beta_{3^2P}^{\mathrm{Li}}$ which is found larger than the $3^2P\rightarrow 3^2D$ transfer coefficient, so that supplementary collisional processes not included in our model must be taken into account.

1. *Excitation transfer towards the 3^2S state*

$$\mathrm{Li}(3^2P)+\mathrm{Li}(2^2S)\rightarrow \mathrm{Li}(3^2S)+\mathrm{Li}(2^2S)+\Delta E$$

with $\Delta E\sim 3700$ cm^{-1}.

Fluorescence starting from the 3^2S state in the $3^2S\rightarrow 2^2P$ transition cannot be observed easily with our experimental set up ($\lambda=8126$ Å). But we can expect a relatively low rate coefficient for this process if we compare with a similar excitation-transfer process studied in helium[15]

$$\mathrm{He}(3^1P)+\mathrm{He}(1^1S)\rightarrow \mathrm{He}(3^1S)+\mathrm{He}(1^1S)+\Delta E(1345\mathrm{cm}^{-1})$$

with a cross section $\sigma\cong 0.1\times 10^{-16}$ cm^2 for $kT\sim 255$ cm^{-1}.

2. *Quenching by* Li_2 *dimers*

The concentration of Li_2 dimers in the lithium vapor varies in the range $1.1\times10^{11}-7\times10^{13}$ cm^{-3} in our experimental conditions. Excitation transfers from the 3^2P atomic state towards an excited state of the dimer

$$Li(3^2P)+Li_2(X^1\Sigma_g^+)\rightarrow Li(n^2L)+Li_2^*$$

with $n\leq3$, can give rise to quenching of the $Li(3^2P)$ state population.

Such a process was observed in Na and Na_2.[28] A rate coefficient of $\sim3.4\times10^{-9}$ cm^3 sec^{-1} for the excitation transfer process

$$Na^*(3P)+Na_2(X^1\Sigma_g^+)\rightarrow Na(3S)+Na_2^*(A^1\Sigma,a^3\pi)$$

was deduced from laser induced fluorescence measurements. Assuming this value for the rate coefficient in lithium, we obtain a quenching coefficient of the 3^2P state in the range $5\times10^3-2\times10^5$ sec^{-1} which is too low by one order of magnitude to account for the observed discrepancy. Nevertheless, a search for such a process in our experiment is now in progress.

3. *Associative ionization*

Associative ionization process may be described as the collisional association of an excited-state and a ground-state atom resulting in the formation of an autoionizing dimer, followed by autoionization into dimer ion plus electron. Since the 3^2P and 3^2D states lie near the bottom of the Li_2^+ potential well[29,30] within ~2000 cm^{-1}, this process is energetically possible for atoms with kinetic energy greater than $\sim3-4$ kT:

$$Li(3^2P)+Li\rightarrow Li_2^+e^--\Delta E\ .$$

With this assumption we can deduce an estimate of the rate coefficient for this process:

$$\beta_{ion}^{Li}\sim\beta_{3^2P}^{Li}-\beta_{3^2P\text{-}3^2D}^{Li}\cong1.8\times10^{-9}\ \text{cm}^3\ \text{sec}^{-1}\ .$$

This value can be compared with the associative ionization rate coefficient of the 3^1D state of helium: 3×10^{-10} cm^3 sec^{-1}.[15]

On the other hand, the associative ionization process appears to be inefficient for the 3^2D state since within the error bar, $\beta_{3^2D}^{Li}=\beta_{3^2D\rightarrow3^2P}^{Li}$.

V. CONCLUSION

Two-step laser excitation of the 4^2S state in lithium followed by radiative cascade populating the 3^2P state and subsequent collisional transfer to the 3^2D state allowed us to determine collisional $3^2P\rightarrow3^2D$ excitation transfer and 3^2P, 3^2D, and 4^2S quenching rate coefficients whereas direct excitation of the 3^2P state cannot be performed.

These rate coefficients and the 3^2P, 3^2D, and 4^2S radiative lifetimes are deduced from the time analysis of the fluorescences using a numerical identification method specially developed for this experiment.

Comparison of our results can only be done with fine-structure-changing collisions in the heavier alkali atoms, but the essential features concerning the respective efficiency of the colliding atoms (Li, He, Ne) are the same.

Excitation-transfer processes within the $n=4$ lithium levels are currently investigated in our laboratory using two-step excitation of the 5^2S level and radiative cascade towards the 4^2P level.

ACKNOWLEDGMENT

The technical assistance of J. C. Pellicer is gratefully acknowledged.

APPENDIX: IDENTIFICATION METHOD

The principle of the identification method is the following: Coefficients A, B, and C, of Eq. (10) are determined so as to minimize the difference between the experimental curves $N_1^{expt}(t)$ and those calculated from the model. This problem is equivalent to that of finding the minimum of the error function

$$J(A,B,C,N_1)=\int_{t_0}^{t_1}(N_1^{expt}-N_1)^2dt\ , \tag{A1}$$

with N_1 solution of

$$g(N_1,A,B,C)=A\frac{d^2N_1}{dt^2}-B\frac{dN_1}{dt}+CN_1-N_3=0 \tag{A2}$$

and

$$N_3(t),N_1(t_0),\left[\frac{dN_1}{dt}\right]_{t_0}$$

given.

The minimum of $J(A,B,C,N_1)$ is obtained when the Hestenes-Powell Lagrangian

$$\mathscr{L}(N_1,A,B,C,p)=J(A,B,C,N_1)+\int_{t_0}^{t_1} pg(N_1,A,B,C)dt \quad \text{(A3)}$$

is minimum with respect to N_1.[31,18]

In Eq. (A3) p is a Lagrange multiplier vector. The functional derivative $\partial\mathscr{L}/\partial N_1$ is easily calculated and the minimum condition $\partial\mathscr{L}/\partial N_1=0$ is written as

$$A\frac{d^2p}{dt^2}+B\frac{dp}{dt}+C_p=2(N_1^{\text{expt}}-N_1)\ , \qquad p(t_1)=0\ , \quad \left[\frac{dp}{dt}\right]_{(t_1)}=0\ , \quad \text{(A4)}$$

where $p(t)$ appears to be the solution of the adjoint problem.[32] With $p(t)$ being the solution of Eq. (A4), the functional derivation of the error function (gradients) is given by the scalar product of p with the A, B, and C, derivatives of $g(N_1,A,B,C)$ considered as vectors:

$$\frac{\partial J}{\partial A}=\int_{t_0}^{t_1} p\frac{d^2N_1}{dt^2}dt\ ,$$

$$\frac{\partial J}{\partial B}=-\int_{t_0}^{t_1} p\frac{dN_1}{dt}dt\ ,$$

$$\frac{\partial J}{\partial C}=\int_{t_0}^{t_1} pN_1dt\ .$$

These values are used in the iterative gradient algorithm (Eq. 11) to compute the coefficients A^{id} B^{id}, and C^{id} yielding $J(A, B, C, N_1)$ minimum.

The iterative process is stopped when

$$J\Big/\int_{t_0}^{t_1} N_1^2dt<\epsilon\ ,$$

where ϵ is a given relative error (typically $0.001<\epsilon<0.01$). As explained in the case of the first-order identification method,[15] the total errors ΔA^{id}, ΔB^{id}, and ΔC^{id} including numerical and experimental noise and errors are estimated by varying the experimental values $N_1^{\text{expt}}(t)$ within their error bars.

The first approximation A°, B°, and C° that is needed to start the gradient algorithm is computed from least-square resolution of the overdetermined linear system

$$A^\circ\ddot{N}_1(t_i)-B^\circ\dot{N}_1(t_i)+C^\circ N_1(t_i)=N_3(t_i) \qquad i=0,\ldots,n\ ,$$

where $\ddot{N}_1(t_i)$, $\dot{N}_1(t_i)$ are, respectively, the second and first derivatives of N_1 calculated from the experimental curves at different times $t_i=t_0,\ldots,t_n$. Generally, only crude estimates of $\ddot{N}_1(t_i)$, $\dot{N}_1(t_i)$ can be obtained from experimental noisy data, so that A°, B°, and C° must only be used as a first approximation.

[1]M. Krauss, P. Maldonado, and A. C. Wahl, J. Chem. Phys. 54, 4944 (1971).
[2]W. E. Baylis, J. Chem. Phys. 51, 2665 (1969).
[3]J. Pascale, and J. Vandeplanque, J. Chem. Phys. 60, 2278 (1974).
[4]J. Cuvellier, P. R. Fournier, F. Gounand, J. Pascale, and J. Berlande, Phys. Rev. A 11, 846 (1975).
[5]J. M. Mestdagh, J. Cuvelier, J. Berlande, A. Bivet, and P. DePujo, J. Phys. B 13, 4589 (1980).
[6]M. Glodz, J. B. Atkinson, and L. Krause, Can. J. Phys. 59, 548 (1981).
[7]M. Hugon, F. Gounand, P. R. Fournier, and J. Berlande, J. Phys. B 13, 1585 (1980).
[8]T. F. Gallagher, S. A. Edelstein, and R. M. Hill, Phys. Rev. A 15, 1945 (1977).
[9]J. Eldward-Berry, and M. Berry, J. Chem. Phys. 72, 4500 (1980).
[10]C. R. Vidal, and J. Cooper, J. Appl. Phys. 40, 3370 (1969).
[11]L. A. Melton, and P. H. Wine, J. Appl. Phys. 51, 4059 (1980).
[12]K. G. Ibbs, P. H. Wine, K. J. Chung, and L. A. Melton, J. Chem. Phys., 74, 6212 (1981).
[13]A. N. Nesmayanov, *Vapor Pressure of the Chemical Elements* (Elsevier, Amsterdam, 1963).
[14]T. J. McIlrath, and J. L. Carlsten, J. Phys. B 6, 697 (1973).
[15]B. Dubreuil, and A. Catherinot, Phys. Rev. A 21, 188 (1980).
[16]W. L. Wiese, H. W. Smith, and B. M. Glennon, Natl. Stand. Ref. Data Ser., Natl. Bur. Stand. 1, 4 (1966).
[17]A. Catherinot, and B. Dubreuil, Phys. Rev. A 23, 763 (1981).
[18]J. Cea, *Optimisation: Théorie et Algorithmes* (Dunod, Paris, 1971).
[19]J. Heldt, and G. Leuchs, Z. Phys. A 291, 11 (1979).
[20]D. Schulze-Hagenest, H. Harde, W. Brand, and W. Demitroder, Z. Phys. A 282, 149 (1977).
[21]W. Nagourney, W. Happer, and A. Durio, Phys. Rev. A 17, 1394 (1978).
[22]F. Biraben, K. Beroff, G. Grynberg, and E. Giacobino, J. Phys. (Paris) 40, 519 (1979).
[23]P. W. Pace, and J. B. Atkinson, Can. J. Phys. 52, 1635 (1974).
[24]P. Münster, and J. Marek, J. Phys. B 14, 1009 (1981).
[25]M. Pimbert, J. Phys. (Paris) 33, 331 (1972).
[26]I. Siara, E. S. Hrycyshyn, and L. Krause, Can. J. Phys. 50, 1826 (1972).

[27]L. Krause, Appl. Opt. 5, 1375 (1966).
[28]L. K. Lam, T. Fujimoto, and A. C. Gallagher, J. Chem. Phys. 68, 3553 (1978).
[29]D. D. Konowalow, and M. E. Rosenkrantz, Chem. Phys. Lett. 61, 489 (1979).
[30]W. A. Young, M. Y. Mirza, and W. W. Duley, Opt. Commun. 31, 157 (1979).
[31]M. R. Hestenes, J. Optim. Th. Appl. 4, 303 (1969).
[32]J. Delforge, Appl. Math. Comp. 2, 311 (1976).